Finite element modeling and analysis of ultrasonic bonding process of thick aluminum wires for power electronic packaging

Tang, Jiuyang ; Li, Liangtao ; Zhang, Guoqi; Zhang, Jing ; Liu, Pan

DOI
10.1016/j.microrel.2022.114859

Publication date
2022

Document Version
Final published version

Published in
Microelectronics Reliability

Citation (APA)
Tang, J., Li, L., Zhang, G., Zhang, J., & Liu, P. (2022). Finite element modeling and analysis of ultrasonic bonding process of thick aluminum wires for power electronic packaging. *Microelectronics Reliability*, *139*, Article 114859. https://doi.org/10.1016/j.microrel.2022.114859

Microelectronics Reliability 139 (2022) 114859

Contents lists available at ScienceDirect

Microelectronics Reliability

journal homepage: www.elsevier.com/locate/microrel

Finite element modeling and analysis of ultrasonic bonding process of thick aluminum wires for power electronic packaging

Jiuyang Tang [a], Liangtao Li [a], Guoqi Zhang [b], Jing Zhang [c], Pan Liu [a,d,e,*]

[a] Academy for Engineering and Technology, Fudan University, Shanghai, China
[b] Electronic Components, Technology, and Materials, Delft University of Technology Delft, the Netherlands
[c] Heraeus Materials Technology Shanghai Ltd., Shanghai, China
[d] Yiwu Research Institute of Fudan University, Yiwu, China
[e] Research Institute of Fudan University in Ningbo, Ningbo, China

ARTICLE INFO

Keywords:
Thick aluminum wire
Ultrasonic wedge bonding
Finite element analysis
Numerical analysis
Power electronic packaging

ABSTRACT

Ultrasonic wedge bonding of aluminum (Al) wires is a widely applied interconnect technology for power electronic packaging. The joint quality of the wedge bonding is mainly affected by the process parameters and material properties. Inappropriate process parameters will lead to failure modes such as chip surface pit, metal layer peeling off, wire cracking, non-sticking to the pad, etc., which limits the long-term stability of power devices. In order to reach the desired reliability, the design of experiment (DoE) is generally deployed which is costly in terms of time and related materials. Therefore, simulation-assisted analysis is in demand to rapidly narrow down the process windows. In this paper, an ultrasonic bonding model involving thick Al wires (300 μm) was established based on the Finite Element Method (FEM), to optimize process parameters effectively with reduced time and cost. The model was designed in ANSYS utilizing the transient structural mechanics module with various stresses and ultrasonic power, to simulate the relative deformation of the bonded wires and the displacement against the substrate. The result was then verified by ultrasonic wedge bonding samples with 9 sets of process parameters. The stress distributions were simulated and analyzed with the failure modes of tensile strength tests, while the deformation of wires under various process parameters was measured and compared with shear strength tests. Further, the relationship between the failure modes of the joint and the deformation was then analyzed by Response Surface Method (RSM), and the regression equation of the wire deformation and related process parameters was established and fitted with the actual sample's data. Such analysis not only found the optimum range of the deformation of thick Al ultrasonic wire bonds but also quickly provided a range of optimized processes for Al thick wires applying ultrasonic wedge bonding techniques.

1. Introduction

The popularization of renewable energy is driven by the application of power electronics, such as wind, solar, electric vehicles, rail transportations, industrial control, etc. [1]. With the increasing demand for power electronics, power semiconductor packaging received more and more attention towards higher power density, smaller packaging, and lower power consumption [2]. Meantime, high operating temperatures and high voltage applications promote the need for reliability [3]. In a power device packaging system, bonding wires appear to be the most easily degraded by electrical, mechanical, and thermal stresses [4], which present challenges for the reliable design of power electronic packages.

For power electronics, thick bond wires, with diameters ranging from 200 μm to 600 μm, are commonly used for high current density applications. Ultrasonic wedge bonding to connect thick bond wires with chips and substrates is under development [5]. In order to improve joint quality, mechanisms of ultrasonic wedge bonding have been studied for several years. Early speculations believed that friction promotes the generation of heat that melts wires and stable joints form after cooling [6]. However, it was challenged by more recent studies which believed that the ultrasonic energy eliminates the oxide layer at the metal interfaces and consequently activates the metals in contact [7]. Further, due to the loss of oxide layer protection, metal atomic diffusion occurs on the interface, forming the dense bonding joints [5,8,9]. Generally, such bonding force and ultrasonic power are usually higher

* Corresponding author at: Academy for Engineering and Technology, Fudan University, Shanghai, China.
E-mail address: panliu@fudan.edu.cn (P. Liu).

https://doi.org/10.1016/j.microrel.2022.114859
Received 14 May 2022; Received in revised form 10 August 2022; Accepted 1 November 2022
Available online 14 November 2022

than counterparts in thin bond wire processing (e.g. ball bond). For the bonding process, it is essential to use suitable parameters. Excessive wire deformations lead to bonding tools wearing out, substrate/chip damage, stress/fracture of bonding joints, etc. while insufficient wire deformations bring failures of non-sticking to the pad, metal layer peeling off, etc. These problems increase the failure rate and affect the availability and optimal operation planning of the entire power system [10]. Several trade-offs cannot be solved easily. For improvement, it is complicated to optimize the wire deformations since it is influenced by various factors such as wire material, process parameters, substrate coating, and chip coating. Among all the process parameters, ultrasonic power and bond force are chosen as control factors, for the reason they can directly influence wire deformations. In general, such parameter optimization usually requires a design of experiment (DoE) which would result in hundreds of samples, together with many wasted chips and substrates.

Therefore, high-accuracy modeling for evaluating the effects of the ultrasonic wedge bonding process is in demand. Benefit from the efficiency of simulation, components of different geometries can be repeated. Such simulation requires an in-depth understanding of packaging materials, key processes, and influential parameters. So far, relevant studies are mainly focused on the mechanical and microstructure properties of thick aluminum (Al) bonding wires [11–13], reliability tests containing thermal cycling, power cycling, and other accelerated lifetime tests (ALT) [14], etc. Meanwhile, with the support of finite element simulations [11,15], the fatigue behavior related to the material properties in the thick bonding wires was investigated in detail [16,17]. A large number of failure modes were recorded to provide the basis for bond wire aging assessments [17], comparative analysis of aging mechanisms, and ALT. Fatigue lifetime was found to be influenced by wire diameter [18], junction temperature swing [14], monitoring current [14], aspect ratio of the wedge, etc. [11]. It is clear that parameters of the process are key factors affecting the reliability of thick Al wire bonding. [19,20].

The finite element analysis model with DoE was used to study the influence of bonding parameters, chip pads, inclination issues [21], and wedge deformation effect on-chip damage [22]. In general, the quality of bonding adhesion is regarded as the basis for determining reliability, which is linked to the shear strength tests. In the simulation, the contact and displacement behavior between the wire and the substrate were observed [23,24], it's also convenient to achieve stress distribution and force analysis. In addition, bond reliability is focus on factors such as friction [25,26], dynamic behavior [27], ultrasonic frequency [24], deformation, etc. [12]. Proper simulation design can analyze bond formation in detail, further, it can help to process improvement. However, few pieces of research were focused on using FEM to analyze process parameters that influence reliable thick Al bond wires.

In this paper, a finite element process model was established to adapt the process parameters of bonding force and ultrasonic power by combining simulation with reliability tests, which quickly narrowed the process windows for thick bond wires on power devices packaging. The process model was firstly designed to simulate the deformation of thick Al bond wires. Then, the deformation and equivalent plastic strain of the wire were examined and compared. Such models were further verified by bonding experiments on Ag-coated direct bonded copper (DBC) substrates, using deformation on tensile and shear tests as the evaluation of bonding qualities. With respond surface method (RSM) analysis, the regression equation of the wire deformation and related process parameters was established and fitted with the actual samples' data. Such analysis provided an optimized process window for Al thick wire bonds while enabling ultrasonic wedge bonding techniques. In the end, the optimum range of the deformation of thick Aluminum ultrasonic wire bonds was also suggested.

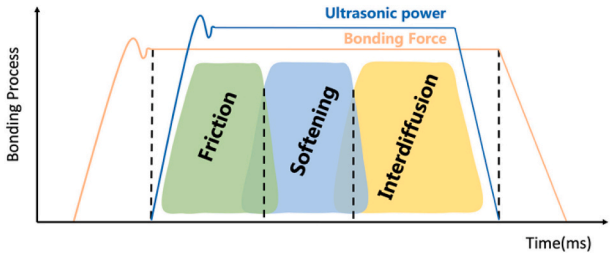

Fig. 1. Schematic of ultrasonic bonding process.

2. Ultrasonic wire bonding simulation model description

2.1. Bonding process modeling

The ultrasonic wire bonding process was divided into three physical coupling processes, as shown in Fig. 1. Firstly, the wire plastically deforms under the force of the tool. Secondly, the tool drives the wire to vibrate at a high frequency in the bonding area. Due to the high-speed friction between the wire and the pad, the oxide layer on the contact surface is fractured. Thirdly, under the effect of ultrasonic power, the wedge part of the wire continuously deforms, and atomic diffusion occurs on the contact interface, forming a stable bonding joint. Based on such analysis, the ultrasonic bonding process was converted into a numerical calculation process by using FEM. Then, the mechanism in the ultrasonic bonding process and the influence of process parameters on the bonding quality were further analyzed.

In the first stage, the tool applies force on the bonding wire towards the pad to make the wire plastically deform. The phenomenon can be described as a stress-strain curve, which obtains the increment of wire diameter $\Delta\varepsilon$ and increment of stress $\Delta\sigma$ during the plastic deformation. T in Eq. (1) is the tangent modulus of material at a plastic stage, which is equivalent to the slope of the second section of the curve in the simplified stress-strain function.

$$\Delta\sigma = T\Delta\varepsilon \tag{1}$$

As the wire deforms, the contact plane between it and the tool expands, while the stress drops rapidly. The deformation of the wire conforms to the elastic deformation equation, and the deformation and external force follow Hooke's Law as Eq. (2).

$$\sigma = E\varepsilon \tag{2}$$

while σ is the stress on the surface. E is the elastic modulus, and ε is the strain produced on the surface. A smooth stress-strain curve is described as the stress increases until the wire deforms irretrievably and Hooke's law fails. In order to accelerate the calculation of the ultrasonic bonding model, the stress-strain constitutive model of bonded wires was simplified to a bilinear elastic-plastic strengthening model in finite element analysis.

The deformation process of the bonding wire and pad is related to the load stress, corresponding to the nonlinear characteristics of the material. Therefore, the solution of the nonlinear finite element equation described the wire deformation as a limited incremental interval, where the deformation can be linearized. Then the iterative method is used to restore all linearization processes to the nonlinear. Eq. (3) is the incremental expression of the stress-strain constitutive equation of the wire.

$$\Delta\sigma_{ij} = D^{ep}_{ijkl}\Delta\varepsilon_{kl} \tag{3}$$

While $\Delta\varepsilon_{kl}$ represents the strain increment at kl, $\Delta\sigma_{ij}$ represents the stress increment at ij, hence D^{ep}_{ijkl} represents the modulus at kl versus ij. The equation describes the relationship between stress and strain increment at the stage of nonlinear wire deformation, which is related to the change of load force. Ultrasonic vibration system controls the joint quality by adjusting the vibration of the bond tool, and the value of

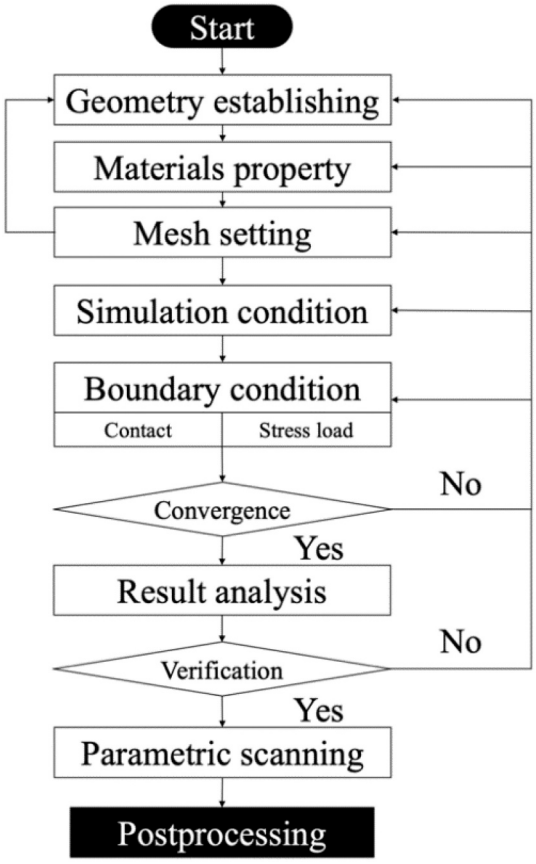

Fig. 2. Workflow of finite element analysis.

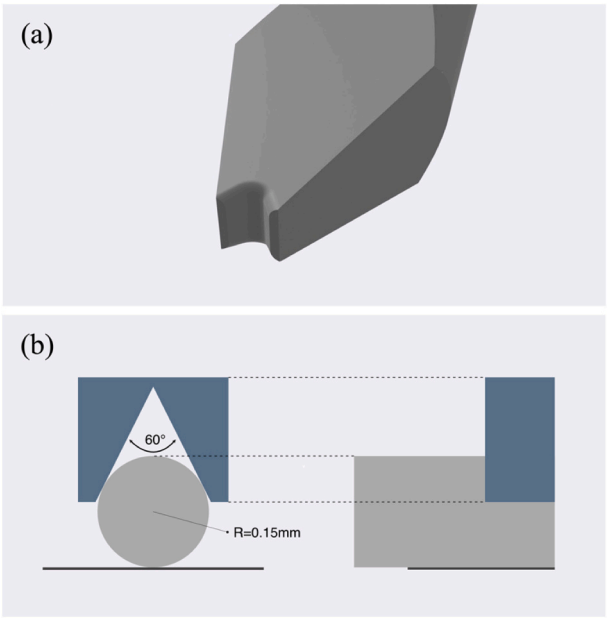

Fig. 3. (a) Shape of bonding tool. (b) Schematic of wire bonding model.

ultrasonic power correspond to the sound intensity I. The math between them follows Eq. (4).

$$I = 1/2\rho c\omega^2\xi^2 \quad (4)$$

where ρ is the density of the material; c is the velocity of ultrasonic wave propagation; ω is angular frequency; ξ is the ultrasonic amplitude. In the equation, ultrasonic power value, frequency, and amplitude show quadratic correlation. Therefore, in the design of simulation, the adjustment of ultrasonic power is equivalent to the control of ultrasonic frequency and ultrasonic vibration amplitude.

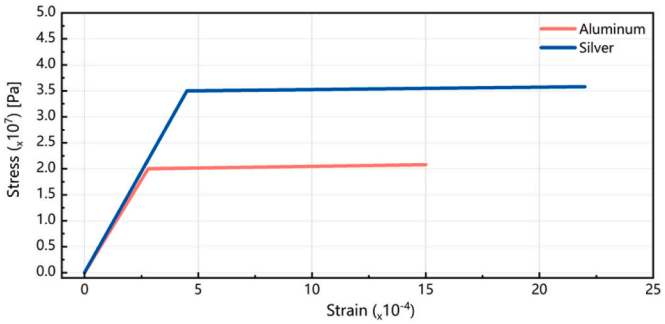

Fig. 4. Stress-strain curve of materials in ANSYS.

Table 1
Material properties.

Materials	Al	Ag	AlN	Steel
Density (kg/m^3)	2689	10,491	3300	1450
CTE (ppm/K)	24.5	19.6	4.6	12
Young modules (GPa)	70	76	320	400
Poisson coefficient	0.33	0.37	0.24	0.3
Yield limit (MPa)	20	35	/	/
Tangent modulus (MPa)	700	760	/	/
Hardening model	BIH	BIH	LP	LP

2.2. Bonding simulation method

Commercial software ANSYS provided integrated functionality to compute structural mechanic problems by using FEM to solve partial differential equations. In this paper, ANSYS Workbench 19.0 with transient structural mechanics module was applied. Starting with the definition of initial and boundary conditions for the mesh geometry and differential problems of the model, the workflow of transient simulation followed the iterative scheme shown in Fig. 2.

The geometry of the bonding tool from K&S Ltd. was shown in Fig. 3 (a). Using 2D structure as a finite element model can simplify the calculation and improve the convergence quality of nonlinear problems. Therefore, major components such as tools, Al wires, pads, and chips were modeled, excluding solder layers and chip interfaces, to focus on the wire deformations. The substrates only exhibited deformation properties limited to the elastic domain to prevent unexpected deformations. A geometric model was established as shown in Fig. 3(b), where the opening angle of the wedge tool was 60° and the model of the thick Al wire was a cylinder with a diameter of 300 μm. The pad was a rectangular panel of only 4 μm. Through the physical geometric design, a complete analysis model was established to analyze the overall deformation and stress distribution in post-processing.

The strengthening models of stress-strain curves vary by material. For components (Al wires and silver covered pads) that were under plastic deformation in the simulation process, a bilinear strengthening model was adopted to be equivalent to the stress-strain curves of Al wires and silver pads. Fig. 4 showed the simplified curves of Al and silver used in the finite element model. The slope of the first step represented the young's modulus of the corresponding material, and the stress at the turning point was the yield strength. The second slope was the tangent modulus, which was usually one-hundredth of Young's modulus. Such a linear elastic model was used to describe the stress-strain curves of the materials (tungsten steel tool and substrate) which only have elastic

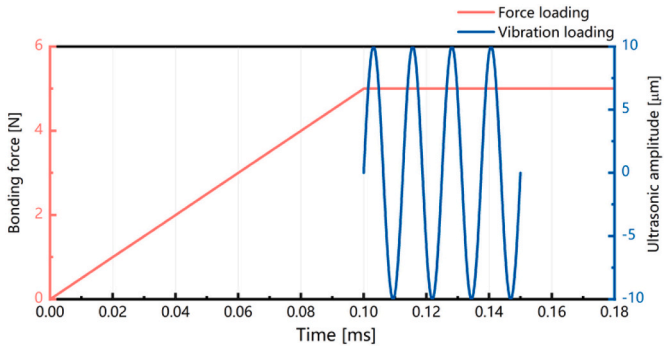

Fig. 5. Loading curve of ultrasonic vibration displacement of bonding tool.

Table 2
Parameter of bonding force and ultrasonic power amplitude.

Group	Bonding force (N)	Amplitude of ultrasonic power (μm)
1	24	10
2	24	15
3	24	20
4	32	10
5	32	15
6	32	20
7	40	10
8	40	15
9	40	20

deformation during the simulation. In ANSYS, the elastic modulus was commonly adopted to define the linear elastic model.

Since the bonding process run fast, changes in material parameters caused by temperature rise in a short period friction were neglected. The parameters of each material at room temperature are shown in Table 1. The material of the tool was tungsten steel, which had a high Young's modulus, hence a rigid body was used to simulate the mechanical behavior of tool bonding. The Al wires were from Heraeus Ltd., 300 μm in diameter, and the pad material was made of silver coating, which will be slightly deformed when squeezed by the metal wire during bonding. Refer to common packaging solutions, the substrate used aluminum nitride ceramic (AlN).

In the definition of boundary conditions and mechanical loads, each non-contact boundary of the model was constrained. Besides, there was a contact coupling between the tool and the wire. In the process, the relative displacement was far less than the wire size, hence, the friction coefficient was regarded as a minor factor in this node. Contact coupling also formed between the wire and the pad. Therefore, according to the selection principle of the Target and Contact in coupling, we set the convex surface of the wire as the Contact, the interface on top of the wire and the pad plane as the Target. When the ultrasonic energy was applied, a relative offset occurred between the wire and pad, therefore, the friction behavior needed to be set in the simulation, and the friction coefficient between the two components was defined as 0.2.

The parameters that affect the morphology of bonding joints were bonding force and ultrasonic power. In the simulation, the force load and displacement load were regarded as equivalent factors. Hence, the simulation scheme of ultrasonic power was achieved by loading time-dependent displacement behavior on the side of the bonding tool.

$$D = 10^{-5} * sin\left(1.6\pi * 10^{5}\left(t - 10^{-4}\right)\right) \quad (5)$$

The displacement load was a time-dependent function, and its mathematical expression was shown in Eq. (5) above. Stress loading A was implemented on the tool towards the substrate, it raised linearly until 0.1 s and maximum to 5 N. The curve of displacement load B is a sinusoidal curve with time, describing the ultrasonic action of the load on the tool. The sine function with a frequency of 80 kHz and an amplitude of 10 μm was set. It will be loaded on the tool after 0.1 ms. And the operation time was 0.05 ms. As the Stress and displacement load application scheme shown in Fig. 5.

Bonding force and ultrasonic vibration amplitude were two main parameters affecting bonding quality. In order to explore the correlation between ultrasonic bond quality and parameters. In the simulation, the bonding force and ultrasonic vibration amplitude were changed as the variables affecting the bonding results. According to the ultrasonic frequency parameters of the K&S bonding machine, when the ultrasonic vibration frequency was 80 kHz, samples will be divided into 9 groups as shown in Table 2.

2.3. Simulation mesh method

The mesh build is important to the simulation results, as shown in Fig. 6. Specifically, fine mesh subdivides the areas of bonding wires and pads which lead to large deformation, while the rest regions are roughly meshed to accelerate the simulation process.

3. Results of simulation

The deformation and equivalent stress distribution of the first bonding joints were similar with the second. They were generally

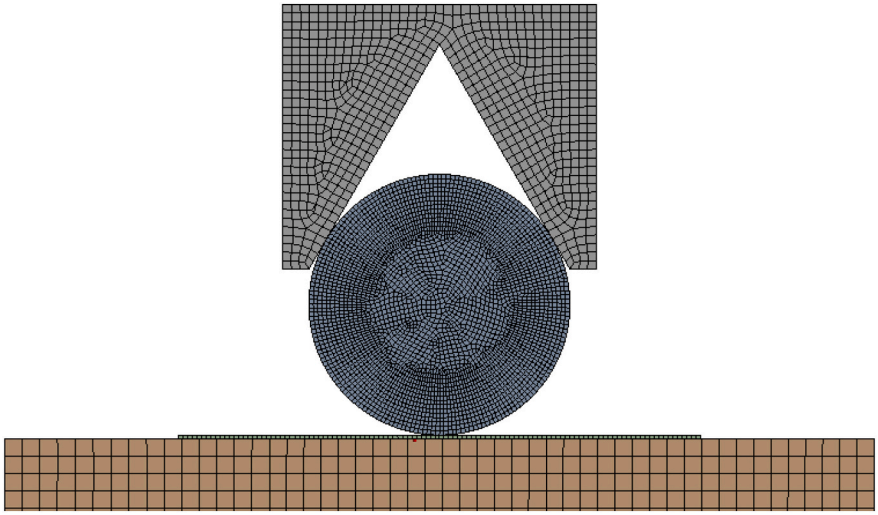

Fig. 6. Mesh setup of the finite element model.

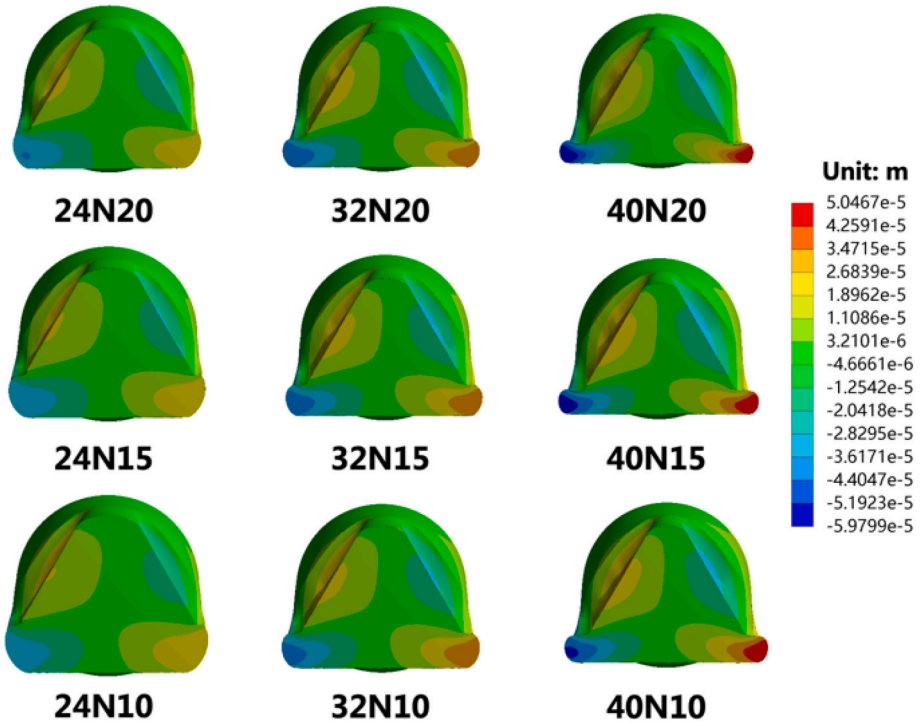

Fig. 7. Comparison of wire bond deformation under different process parameters.

considered to have identical properties and qualities under the same process conditions. The simulation results of deformation and stress can be used to evaluate the stress and mechanical behavior of the wires.

It was clear from Fig. 7 that the deformation of the bonding region was positively correlated with the bonding force and ultrasonic amplitude respectively. It was also illustrated from Fig. 8 that force has a more significant influence on simulation results, while the increase of vibration amplitude did not show obvious deformation effect of wire.

Within the same group, the equivalent stress distributions on the bond wires were compared and plotted from a top view, as shown in Fig. 8(a). High stress distributions were found to be concentrated at the large deformation region of the bonding joint, which was the edge of the tool-wire interface. This was consistent with the positive correlation of stress and strain in plastic deformation. There were no obvious differences in the maximum stress of the simulation results, and it demonstrated that the maximum stress changed little with the increase of bonding force and ultrasonic vibration amplitude. This was because the curve in the plastic deformation stage was flat (the elastic modulus was about 100 times the tangent modulus), therefore, the increase of stress corresponded to the sudden change of strain, and the effect of deformation on the equivalent stress was insignificant. The stress peak occurs at the geometric end of the tool section (the unchamfered edge of the tool) and it did not contribute to the bond formation process. Therefore, the stress at this position was not recorded, and the stress distribution inside the wire after bonding was mainly studied, which provided support for analyzing the reliability of Al wire bonding joints.

The wire section, which represented the stress distribution inside the wire and was far away from the tool section, was selected as the analysis target. Independent of the process parameters, the von-Mises stress in the bonding region was mainly distributed at the bottom near the pad, indicating the potential failure of the region. The stress applied by the reliability test was sustained in the region, which induced the generation and propagation of several cracks. Such stress concentration at the bottom was related to the maximum force exerted by the tool. The downforce of the tool at the inclined surface was dispersed by the angle of the inclined surface. Therefore, the surface was subjected to a small extrusion effect of the tool, on which the stress will not be concentrated. With the increase of ultrasonic power and tool force, the deformation of wire was intensified and more stress was concentrated in the bottom.

A total of 9 combinations of ultrasonic power of 10, 15, 20 and force of 24 N, 32 N, 40 N were selected to carry out DoE. Fig. 9 showed the relationship between wire deformation and bonding time in the simulation model. According to the bonding force, the process parameter combination was divided into three groups. Early dominance was provided by downforce. It showed that at 0–0.1 ms, the Al wire was only subjected to the downforce of the bonding tool, and followed the deformation law at the period. After 0.1 s, ultrasonic vibration had a significant effect on the deformation of Al wire.

Under the condition of constant bonding force, the tangent modulus of Al wire decreased as the deformation of wire increased. According to the ultrasonic bonding mechanism, the wire was in contact with the pad and was alternately affected by two frictional forces in opposite directions. The action of friction made the atoms in the metal wire diffuse, and further forming wedge bonding with accumulated dislocations. The variation of wire deformation with time corresponded to four cycles of ultrasonic vibration. It can be seen that with the increase of ultrasonic time, the effect of each cycle on the shape variable gradually decreased, and the effect of ultrasonic time on the deformation of wire had a marginal effect.

4. Analysis of wire bonding samples

4.1. Ultrasonic bonding experiment of thick Al wire

The deformation of the bonding joint was related to the bonding quality, and there may also be a coupling effect caused by the process parameters. DoE was used to plan the experiment and analyze the bonding joints with reliable quality. The width to diameter ratio θ of the bonding joint should be within a fixed range. To determine the range of θ, wire samples were tested for adhesion reliability. The K&S Asterion series wedge bonding machine was used in the experiment, and the rated ultrasonic vibration frequency was 80 kHz. The tensile strength and shear strength of the samples were tested by the TRY MFM1200 micro-welding spot strength testing machine.

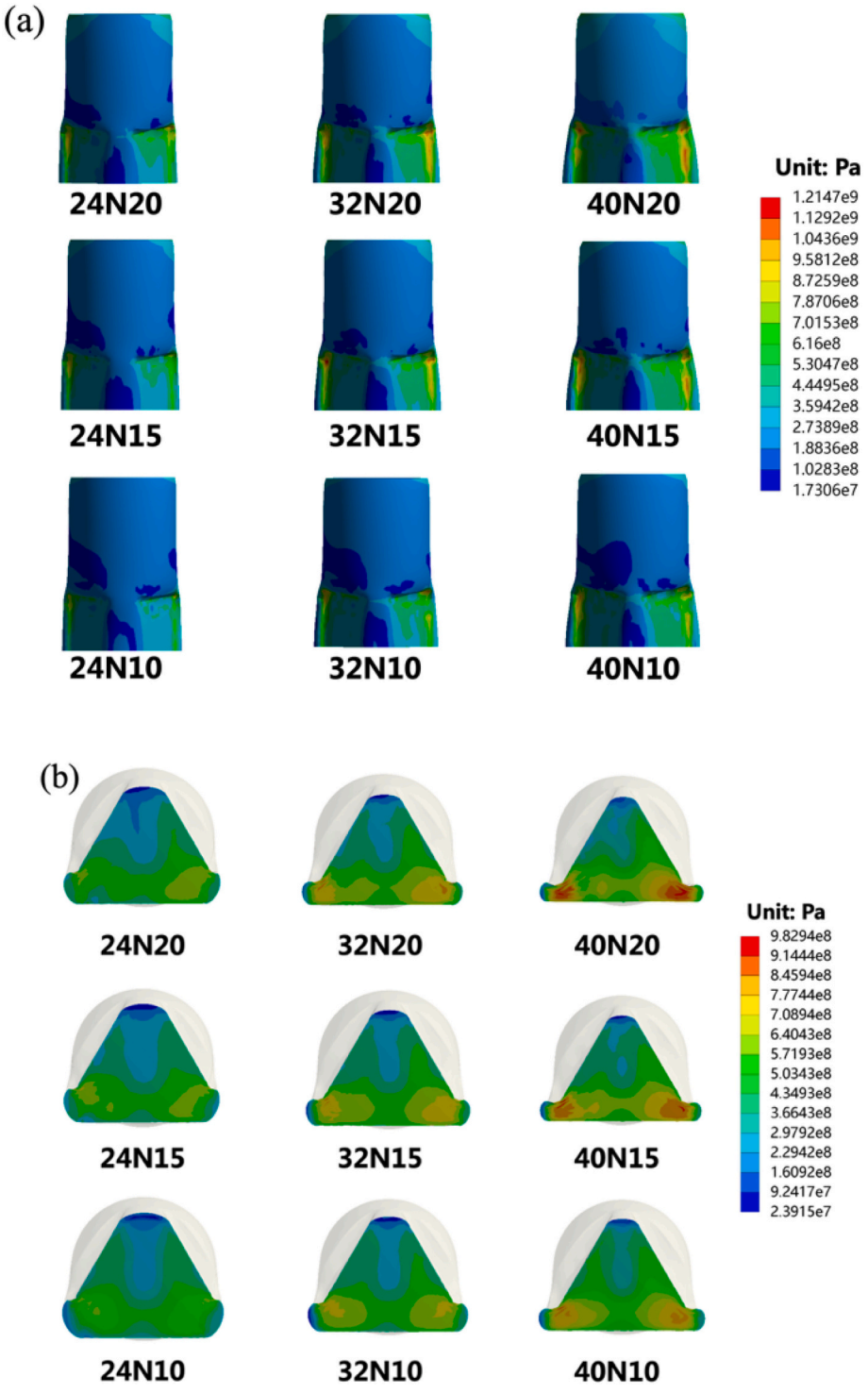

Fig. 8. Comparison of wire bond stress distribution under different process parameters (a) top view (b) front view.

There were two key factors affecting the quality of bonding joints, one was bonding force and the other was ultrasonic power. Considering the influence of factor number A and factor level number B on DoE experiment number N, as shown in Eq. (6).

$$N = B^A \tag{6}$$

DoE planning of ultrasonic bonding experiment was generated through Minitab. Bonding force Settings were 700, 800, and 900, and ultrasonic power Settings were 40, 50, and 60, respectively, as shown in Table 3. Notice: Bonding force and ultrasonic power in a wedge bonding machine were dimensionless values.

The verification experiment conducted ultrasonic bonding of 300 μm diameter Al wires on a blank silver-coated substrate, and obtained a total of 80 bonding joints by completing 40 times ultrasonic process on the substrates. The sample reference group was produced through the process sequence above, one of which was shown in Fig. 10. The sample will complete wedge deformation measurements, followed by shear force and tensile tests.

The deformation of the wire was measured by Nikon ECLIPSE L200N optical microscope. Fig. 11 showed that the deformation value of

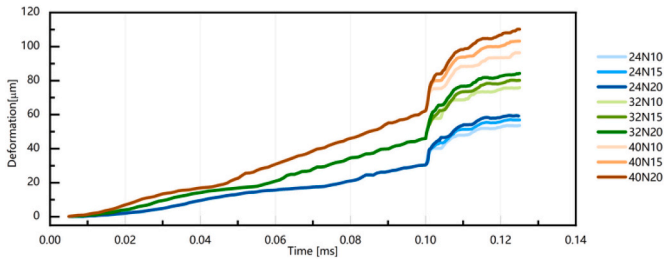

Fig. 9. Deformation value of joint varies with process time.

Table 3
DoE experiment group.

Run sequence	Standard sequence	Bonding force	Ultrasonic bonding power
1	5	800	50
2	7	900	40
3	3	700	60
4	1	700	40
5	6	800	60
6	2	700	50
7	8	900	50
8	9	900	60
9	4	800	40

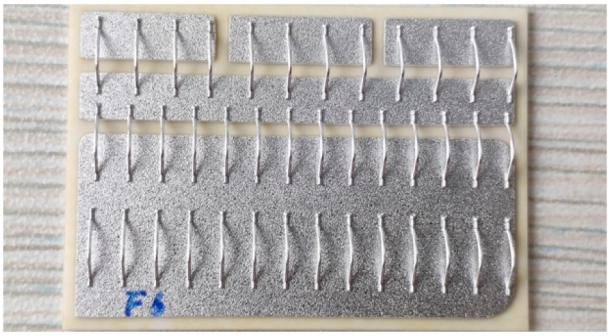

Fig. 10. Sample of bonding process.

bonded wire was measured and marked by post-processing of the measured images at 100 times magnification.

More than 50 measurements from each group of samples were collected and analyzed, and the box plot was drawn as shown in Fig. 12. However, the box graph can only show the discrete distribution of data, and the most accurate statistic to describe the degree of dispersion was the standard deviation. After excluding the abnormal data in each data sample analyzed from the box chart, the mean and variance of each group of wire samples were calculated, as shown in Table 4. It can be seen that within the range of process parameters in this experiment, ultrasonic power had a greater impact on the width of bonding joint forming than tool force. The larger standard deviation of ultrasonic power means that it was more difficult to control the stability and bonding accuracy of the results.

4.2. *Tensile force test*

In the reliability test, the tensile test was applied first, the results of the bonding wire test were recorded and the failure modes were counted, and then the shear strength test was applied to measure the maximum shear force that made the bonding joint peel off to analyze the shear strength. In the tensile test, there were mainly three failure modes, namely knee fracture, leg fracture, and heel fracture, as shown in Fig. 13.

The results showed that all the bonding wires finished the tensile test, and each group of samples was subjected to 40 tests. However, the bonding joints had peeled off 0 times, which indicated that the thick Al wires can produce a stable connection with the substrate after bonding. Knee and leg fractures, both of which were fractured on a non-deformed Al wire. It was inferred that the reason for these two situations was the asymmetry of the tensile force which was related to the strength of the material.

For the heel fracture, referring to the previous simulation results, the equivalent stress was concentrated at the deformation of the tool extrusion wire. As shown in Fig. 14. Affected by the tool structure, the deformation of the heel was irregular, making its diameter smaller than the original wire and became more fragile. In the test, the heel inflection point was the main forced area, which was more prone to cracks or necking.

It can be seen from Fig. 15 that ultrasonic power had a significant influence on the heel fracture of the bonding joints. When the ultrasonic power was 40 and 50, the frequency of it was <10 times. High ultrasonic

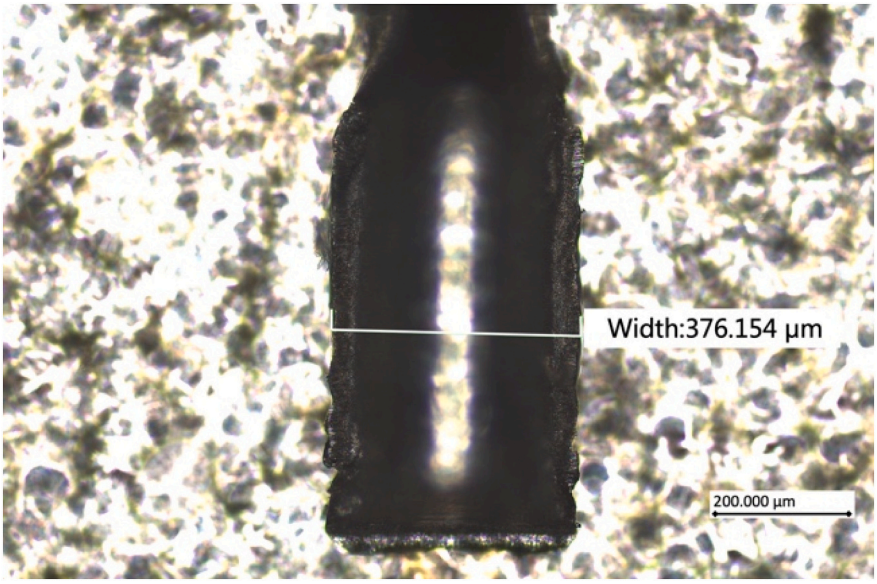

Fig. 11. Width measuring in optical microscope.

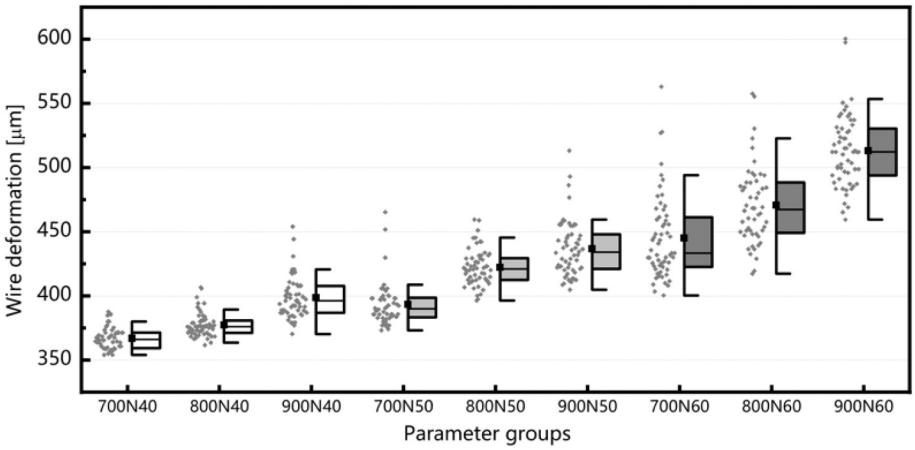

Fig. 12. Width data boxplot of wire bond samples.

Table 4
Mean and variance of joint width of bonding samples.

Group	Ultrasonic bonding power	Bonding force	Mean (μm)	Variance (μm)
1	40	700	366.93	8.52
2	40	800	376.28	7.67
3	40	900	396.76	13.13
4	50	700	390.91	10.91
5	50	800	421.10	12.69
6	50	900	432.74	15.82
7	60	700	440.18	24.81
8	60	800	467.33	25.91
9	60	900	510.14	23.36

energy caused over-bonding, resulting in a large number of failures. However, at low ultrasonic energy, the bonding force was 800, and heel fracture even occurred only once. It showed that the appropriate force had a positive effect on the bonding quality.

At the same time, the maximum force the wire suffered was recorded. As shown in Fig. 16, for the sample group with few heel fracture modes, the deformation of the wire was small, and it was a low probability to fracture at the bonding joint. Therefore, the tensile resistance of the material itself was proved. It can be seen that due to the consistency of the wires in the experiment, the data fluctuate slightly. On the contrary, the sample groups with a large amount of heel fracture modes came from high ultrasonic power groups, the deformation value of the wire was large, and the distribution was random, hence the deformation data appeared discrete. Before reaching the tensile fracture limit of the wire, the heel of it was broken, so the overall maximum tensile strength decreased.

The results showed that the ultrasonic power can greatly increase the deformation of the wire and also the bonding area between the thick Al wire and the substrate. However, it did not play a positive role in the quality of the bonded regions.

4.3. Shear strength test

The shear strength test measured the maximum shear force when the bonding pads on the substrate were completely pushed off under the force of the tool, which was equivalent to the shear resistance of the bonding joints. The data can also indicate the bonding strength of the wire to the metal layer on the substrate. The mean and standard deviation of the maximum shear force data obtained from the analysis of the bond joints were plotted, as shown in Fig. 17.

According to the analysis in the figure, when the ultrasonic power was 50, the corresponding sample bore a large shear force, and the data

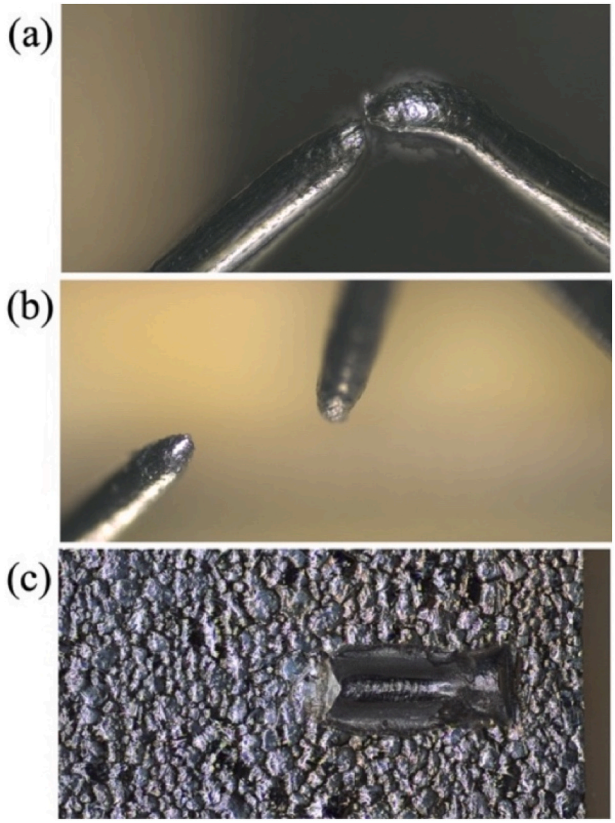

Fig. 13. Failure mode of shear strength test (a) knee fracture (b) leg fracture (c) heel fracture.

was centralized. When the ultrasonic power was 60, the maximum shear force had a good performance, but the bonding quality fluctuated greatly.

After the shear test, traces of wire remained on the substrate. As shown in Fig. 18, the elliptic region of solid lines indicated the wire adhesions to the substrate. This region differed in brightness from the surrounding region due to deformation during bonding. The area of the dotted line represented the residue of the joint. Based on the proportion of residual area, the residual level can be classified into grades 1 to 4 according to 0–25 %, 25–50 %, 50–75 %, and 75–100 %. The higher the grade was, the more sufficient the bond strength was. Sheer grade of 1 and 2 were controlled to be <50 % as a standard for effective bonding.

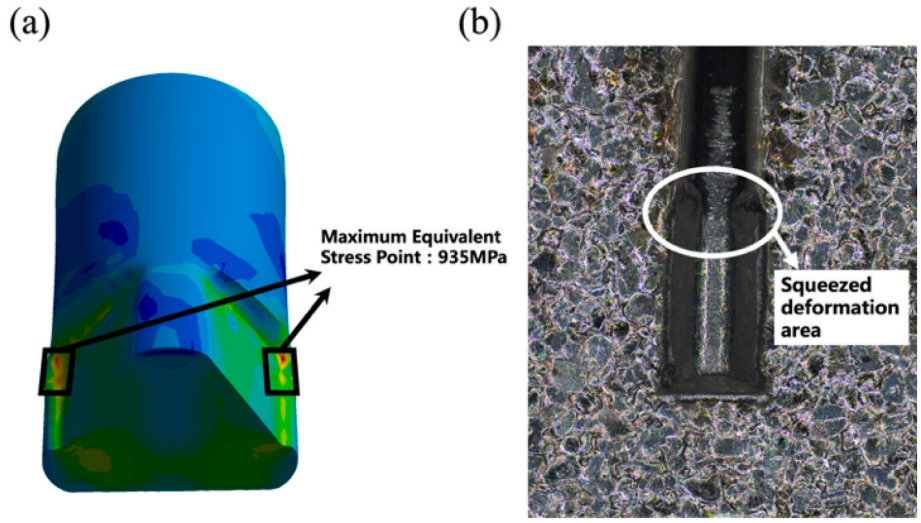

Fig. 14. (a) Stress distribution in FEM simulation (b) top view of bond point.

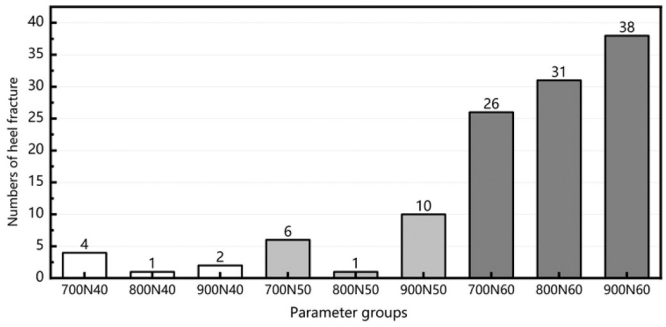

Fig. 15. The number of heel fracture from each group.

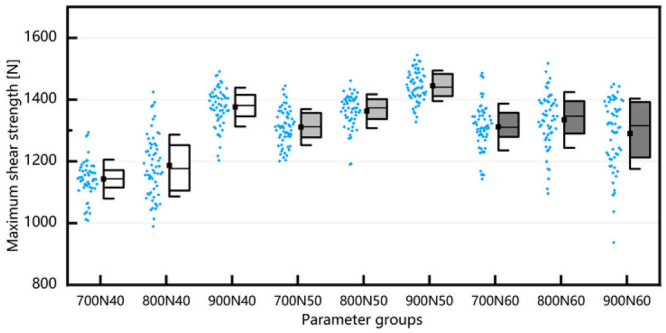

Fig. 17. Maximum shear force under different process.

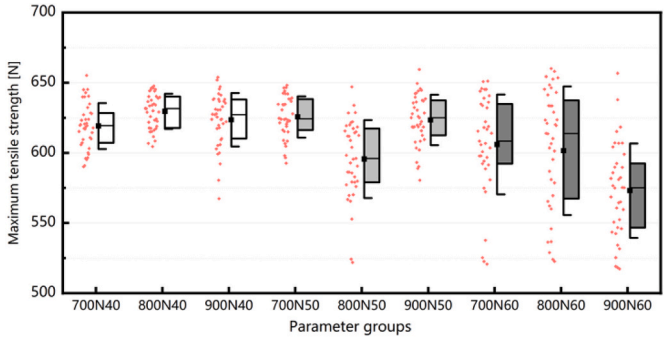

Fig. 16. Maximum tensile force under different process.

4.4. Experimental data analysis and fittings

The central composite design was used to formulate the response surface of the deformation of the bonded wire by analyzing the response of the two factors of bonding force F and ultrasonic power P. The number of wire fractures, mean value of maximum shear force, and standard deviation were sorted out. The response surface diagram between the following response values, bonding force, and ultrasonic power was depicted in Fig. 19. Based on these plots, the value range of the width to diameter ratio θ of the bonding joints can be deduced, and the optimal deformation of thick Al wires in the bonding process can be solved.

By analyzing the response surface of different key values, the parameter combination range of bonding force and ultrasonic power was determined, so that all data points with better measurement performance can be included in this range. Boxed in the figure was the range of process parameters that meet all reliability requirements of the current analysis. This range in Fig. 19 demonstrated that the maximum and minimum deformation can be achieved under the parameter combinations 900 N50 and 700 N45, respectively. The regression equation of bonding joint and process parameters was derived from the deformation data, as Eq. (7) shows. D_e represents the deformation of the bonding joint, F_e is the actual bonding force, and P is the ultrasonic power of the bonding machine.

$$D_e = 511 - 0.016F_e - 11.82P - 0.000156F_e^2 + 0.0842P^2 + 0.01003F_eP \quad (7)$$

The minimum value in this region was 377.711 μm, and the maximum value is 432.741 μm. The width to diameter ratio θ of the bonding joint was calculated to be $1.26 \leq \theta \leq 1.44$. The above results showed that although the increase of ultrasonic power can greatly increase the width of the wire after bonding. In a certain range, ultrasonic power had a positive effect on the reliability of the bonding joint. However, outside the range, the increase of ultrasonic power lead to an opposite result.

The response surface analysis of the simulated deformation data was carried out. After the normalization process, the initial value of the bonding force was set as 300, and the initial value of the ultrasonic power was set as 30. As D_e = 303.61 μm, which approached to the intrinsic diameter of the wire. If the $x = F_e - 300$, $y = P - 30$, when F_e = 300, x = 0; when P = 30, y = 0. According to the test results, the regression equation was introduced to solve the coefficient. Then the

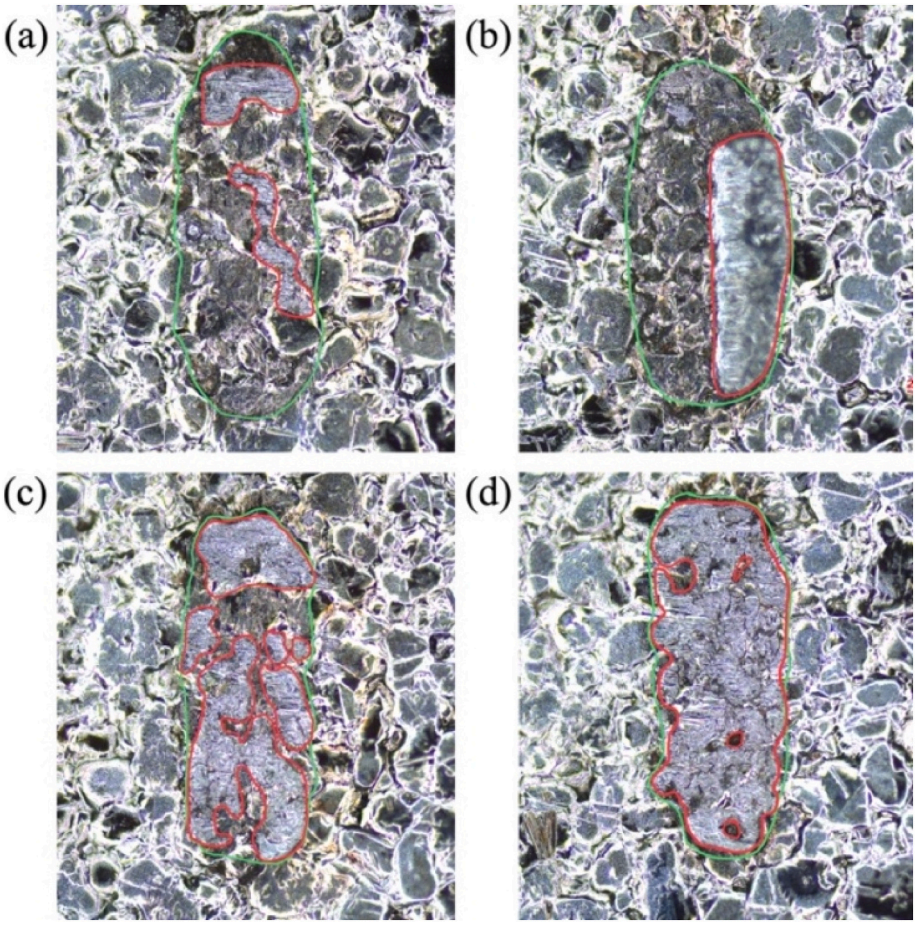

Fig. 18. Schematic of residual level of failed bond joint (a) 0–25 % (b) 25–50 % (c) 50–75 % (d) 75–100 %.

equation between simulated wire deformation and process parameters was obtained, as shown in Eq. (8).

$$D_e = 303.61 - 0.016x - 11.82y - 0.000156x^2 + 0.0842y^2 + 0.01003xy \quad (8)$$

The corresponding relationship between simulation process parameters F_s, A, experimental parameters F_e and P can be found by solving the above system of equations, results as shown in Eq. (9).

$$\begin{cases} F_s = (0.045 + 0.0015(P - 30))(F_e - 300), \\ A = 2.22(P - 30) \end{cases} \quad (9)$$

Fig. 20 showed the comparison between the fitted curve and the simulation curve. When the ultrasonic power was 40 and 50, the deviation of D_s and D_e was controlled within 10 μm, and when the ultrasonic power was 60, the deviation of D_s and D_e was about 15 μm. In the result, the maximum error of the fitting results was 4.5 %.

5. Conclusion

In this paper, the ultrasonic bonding process of thick Al wire was simulated by the FEM. It demonstrated that the maximum stress on the pad appears at the edge of the wedge region by analyzing the simulation data. The application of ultrasonic power can make the stress distribution inside the wire more uniform, and suitable power parameters were more conducive to the formation of bonding joints. In addition, the ultrasonic bonding experiments (ultrasonic wedge bonding samples with 9 sets of process parameters) were designed to verify the model. The stress distributions were simulated and analyzed with the failure modes of tensile strength tests, while the deformation of wires under various process parameters was measured and compared with shear strength tests. Furthermore, the above data were analyzed utilizing the method of RSM. For the 300 μm Al wire bonding joint of the experimental object, the optimal aspect ratio θ was in the range of 1.26 to 1.44. And the regression equation was fitted by analyzing the response surface of deformation data obtained from the FEM. Specifically, by assuming a linear relationship between the simulation and the actual process values, the simulation regression equation of the wire deformation and related process parameters was established with the sample's data, and the mathematical relationship between the parameters was deduced. Finally, the error was optimized within 4.5 %. Simulation and analysis results above can predict the heel fracture of the wire, and at the same time provided a reference for the optimal range of the ratio between the deformation and the original diameter after the bonding process was completed. It also provided a new feasible scheme for rapidly finding the optimal process parameters windows in the actual bonding process.

CRediT authorship contribution statement

Jiuyang Tang: Software, Writing – original draft. **Liangtao Li:** Software, Data curation, Validation. **Guoqi Zhang:** Supervision. **Jing Zhang:** Methodology. **Pan Liu:** Methodology, Supervision, Writing – review & editing.

Declaration of competing interest

All authors disclosed no relevant relationships.

Data availability

The authors do not have permission to share data.

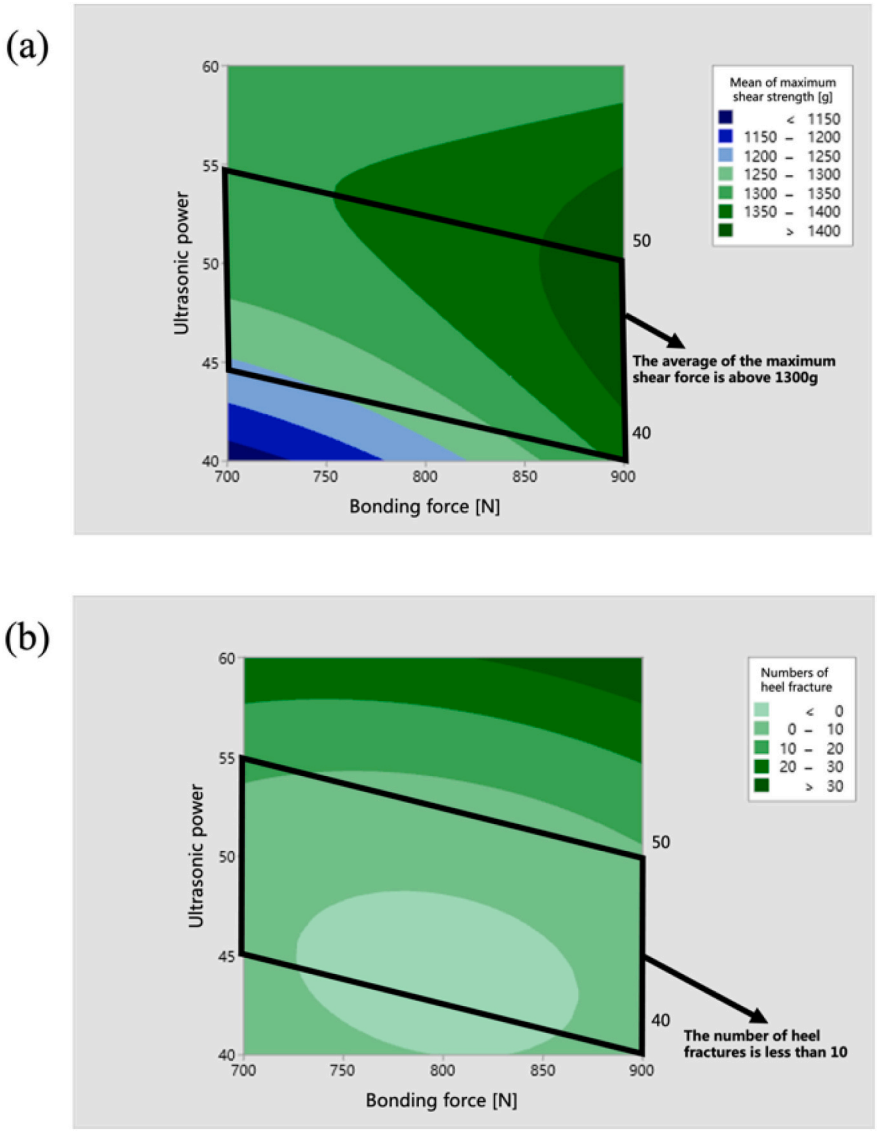

Fig. 19. Contour plot between measurement results and process parameters.

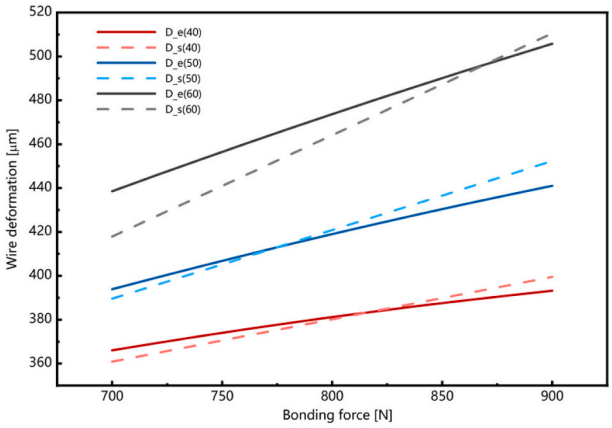

Fig. 20. Optimization results of fit curve.

Acknowledgements

Thank Key-Area Research and Development Program of Guangdong Province (2020B010170002), and Shanghai SiC Power Devices Engineering & Technology Research Center (19DZ2253400) for funding this research and providing simulation support and laboratory accesses. Many thanks to Heraeus Materials Technology Shanghai Ltd. for prototype validation and characterization.

References

[1] S. Peyghami, Z. Wang, F. Blaabjerg, A guideline for reliability prediction in power electronic converters, IEEE Trans. Power Electron. 35 (10) (2020) 10958–10968.
[2] X. She, A.Q. Huang, LÓ, B. Ozpineci, Review of silicon carbide power devices and their applications, IEEE Transactions on Industrial Electronics 64 (10) (2017) 8193–8205.
[3] T. Jiang, R. Rodrigues, U. Raheja, Y. Zhang, Y. Du, P. Cairoli, Overcurrent for aluminum bonding wires in WBG power semiconductors, in: 2019 IEEE 7th Workshop on Wide Bandgap Power Devices and Applications (WiPDA), 2019, pp. 272–276, 29–31 Oct.
[4] Y. Celnikier, L. Benabou, L. Dupont, G. Coquery, Investigation of the heel crack mechanism in Al connections for power electronics modules, Microelectron. Reliab. 51 (5) (2011) 965–974.
[5] Y. Long, J. Twiefel, J. Wallaschek, A review on the mechanisms of ultrasonic wedge-wedge bonding, J. Mater. Process. Technol. 245 (2017) 241–258.

[6] V.H. Winchell, An evaluation of silicon damage resulting from ultrasonic wire bonding, in: 14th International Reliability Physics Symposium, 1976, pp. 98–107, 20–22 April.
[7] G.G. Harman, K.O. Leedy, An experimental model of the microelectronic ultrasonic wire bonding mechanism, in: Proceeding 10th Annual Reliability Physics Symposium, 1972, pp. 49–56.
[8] L. Levine, Wire bonding: the ultrasonic bonding mechanism, Int. Symposium Microelectron. 2020 (1) (2021) 000230–000234.
[9] J.L. Chevalier, D.F. Gibbons, L. Leonard, High-frequency fatigue in aluminum, J. Appl. Phys. 43 (1) (1972) 73–77.
[10] A. Hanif, Y. Yu, D. DeVoto, F. Khan, A comprehensive review toward the state-of-the-art in failure and lifetime predictions of power electronic devices, IEEE Trans. Power Electron. 34 (5) (2019) 4729–4746.
[11] T. Dagdelen, E. Abdel-Rahman, M. Yavuz, Reliability criteria for thick bonding wire, Materials (Basel) 11 (4) (2018).
[12] L. Li, S. Xu, P. Wei, Y.k. Liang, 10 mils Al wire heavy wedge bond wire deformation thickness study, in: 20th International Conference on Electronic Packaging Technology(ICEPT), 2019, pp. 1–4, 12–15 Aug. 2019.
[13] Q. Huang, C. Peng, S.F.M. Ellen, W. Zhu, L. Wang, IEEE transactions on components, Packag. Manuf. Technol. 11 (2) (2021) 212–221.
[14] Y. Huang, Y. Jia, Y. Luo, F. Xiao, B. Liu, Lifting-off of Al bonding wires in IGBT modules under power cycling: failure mechanism and lifetime model, IEEE J. Emerging Sel. Top. Power Electron. 8 (3) (2020) 3162–3173.
[15] N. Miyazaki, N. Shishido, Y. Hayama, Review of methodologies for structural integrity evaluation of power modules, J. Electron. Packag. 143 (2) (2020).
[16] B. Czerny, I. Paul, G. Khatibi, M. Thoben, Influence of wirebond shape on its lifetime with application to frame connections, in: 14th International Conference on Thermal, Mechanical and Multi-Physics Simulation and Experiments in Microelectronics and Microsystems (EuroSimE), 2013, pp. 1–5, 14–17 April 2013.
[17] B. Czerny, G. Khatibi, Interface reliability and lifetime prediction of heavy aluminum wire bonds, Microelectron. Reliab. 58 (2016) 65–72.
[18] L. Merkle, M. Sonner, M. Petzold, Lifetime prediction of thick aluminium wire bonds for mechanical cyclic loads, Microelectron. Reliab. 54 (2) (2014) 417–424.
[19] C. Kaestle, J. Franke, Comparative analysis of the process window of aluminum and copper wire bonding for power electronics applications, in: 2014 International Conference on Electronics Packaging (ICEP), 2014, pp. 335–340, 23–25 April.
[20] B. Czerny, G. Khatibi, Cyclic robustness of heavy wire bonds: Al, AlMg, Cu and CucorAl, Microelectron. Reliab. 88–90 (2018) 745–751.
[21] Y. Liu, Y. Liu, D. Keller, S. Belani, M. Dube, Characterization of Al wire wedge bonding in power electronics package, in: 2012 IEEE 62nd Electronic Components and Technology Conference, 2012, pp. 1893–1898, 29 May–1 June.
[22] H. Zhang, M. Hu, F. Zong, B. Yin, D. Ye, Q. He, Z. Wang, Wafer damage issue study by heavy Al wire wedge bonding, Microelectron. Int. 31 (2) (2014) 129–136.
[23] A. Unger, R. Schemmel, T. Meyer, F. Eacock, P. Eichwald, S. Althoff, W. Sextro, M. Brokelmann, M. Hunstig, K. Guth, Validated simulation of the ultrasonic wire bonding process, in: 2016 IEEE CPMT Symposium Japan (ICSJ), 2016, pp. 251–254, 7–9 Nov.
[24] R. Schemmel, S. Althoff, M. Bro kelmann, A. Unger, M. Hunstig, W. Sextro, "Effects of different working frequencies on the joint formation in copper wire bonding,".
[25] R. Schemmel, T. Hemsel, W. Sextro, "Numerical and Experimental Investigations in Ultrasonic Heavy Wire Bonding,".
[26] Y. Long, J. Twiefel, J. Wallaschek, Contact mechanics and friction processes in ultrasonic wire bonding - basic theories and experimental investigations, J. Sound Vib. 468 (2020), 115021.
[27] Y. Long, F. Schneider, C. Li, J. Hermsdorf, J. Twiefel, J. Wallaschek, Quantification of the energy flows during ultrasonic wire bonding under different process parameters, Int. J. Precis. Eng. Manuf.Green Technol. 6 (3) (2019) 449–463.